

## Electronic and magnetic properties of the graphene–ferromagnet interface

Yu S Dedkov<sup>1,3</sup> and M Fonin<sup>2</sup>

<sup>1</sup> Fritz-Haber-Institut der Max-Planck-Gesellschaft, Berlin, Germany

<sup>2</sup> Fachbereich Physik, Universität Konstanz, Germany

E-mail: [dedkov@fhi-berlin.mpg.de](mailto:dedkov@fhi-berlin.mpg.de)

*New Journal of Physics* **12** (2010) 125004 (22pp)

Received 23 June 2010

Published 13 December 2010


Online at <http://www.njp.org/>

doi:10.1088/1367-2630/12/12/125004

**Abstract.** This paper presents our work on the investigation of the surface structure and the electronic and magnetic properties of the graphene layer on the lattice-matched surface of a ferromagnetic material, Ni(111). Scanning tunneling microscopy imaging shows that perfectly ordered epitaxial graphene layers can be prepared by elevated temperature decomposition of hydrocarbons, with domains larger than the terraces of the underlying Ni(111). In some exceptional cases, graphene films do not show rotational alignment with the metal surface, leading to moiré structures with small periodicities. We discuss the crystallographic structure of graphene with respect to the Ni(111) surface relying both on experimental results and on recent theoretical studies. X-ray absorption spectroscopy investigations of empty valence-band states demonstrate the existence of interface states, which originate from the strong hybridization between the graphene  $\pi$  and Ni 3d valence-band states with the partial charge transfer of the spin-polarized electrons to the graphene  $\pi^*$  unoccupied states. The latter leads to the appearance of an induced magnetic moment of carbon atoms in the graphene layer, which is unambiguously confirmed by both x-ray magnetic circular dichroism and spin-resolved photoemission. Further angle-resolved photoemission investigations indicate a strong interaction between graphene and Ni(111), showing considerable modification of the valence-band states of Ni and graphene due to strong hybridization. A detailed analysis of the Fermi surface of the graphene/Ni(111) system shows very good agreement between experimental and calculated two-dimensional maps of the electronic states around the Fermi level, supporting the idea of spin-filtering. We analyze

<sup>3</sup> Author to whom any correspondence should be addressed.

our spectroscopic results relying on the currently available band structure calculations for the graphene/Ni(111) system and discuss the perspectives of the realization of graphene/ferromagnet-based devices.

 Online supplementary data available from [stacks.iop.org/NJP/12/125004/mmedia](http://stacks.iop.org/NJP/12/125004/mmedia)

## Contents

<b>1. Introduction</b>	<b>2</b>
<b>2. Experimental details</b>	<b>4</b>
<b>3. Results and discussion</b>	<b>6</b>
3.1. Growth and surface structure of graphene on Ni(111) . . . . .	6
3.2. Bonding and magnetism at the graphene/Ni(111) interface . . . . .	8
3.3. Electronic properties of graphene on Ni(111) . . . . .	15
<b>4. Conclusions</b>	<b>19</b>
<b>Acknowledgments</b>	<b>19</b>
<b>References</b>	<b>20</b>

## 1. Introduction

Graphene is a two-dimensional (2D) sheet of carbon atoms arranged in a honeycomb lattice with two atoms in the unit cell [1]–[3]. The  $sp^2$  hybridization between one s orbital and two p orbitals leads to a trigonal planar structure with  $\sigma$  bond formation between the carbon atoms that are separated by 1.42 Å. These bands have a filled shell and hence form a deep valence band. The half-filled  $p_z$  orbitals, which are perpendicular to the planar structure, form the bonding ( $\pi$ ) and antibonding ( $\pi^*$ ) bands. The  $\pi$  and  $\pi^*$  bands touch at a single point exactly at the Fermi energy ( $E_F$ ) at the corner of the hexagonal graphene's Brillouin zone. Close to this so-called Dirac point ( $E_D$ ), the bands display a linear dispersion and form perfect Dirac cones [2]. Thus, undoped graphene is a semimetal ('zero-gap semiconductor'). The linear dispersion of the bands mimics the physics of quasiparticles with zero mass, the so-called Dirac fermions [1]–[3].

The exceptional transport properties of graphene [1] make it a promising material for applications in microelectronics [4, 5] and sensing [6]. This has recently led to a revival of interest in graphene on transition metal surfaces [7]–[18], as large-area epitaxial graphene layers of exceptional quality can be grown, which might be an alternative to micromechanical cleavage for producing macroscopic graphene films. The first mass production of high-quality graphene layers via the chemical-vapor deposition (CVD) method on a polycrystalline Ni surface and its transfer to an arbitrary substrate was demonstrated in the beginning of 2009 [19]. The transferred graphene films showed very low sheet resistance of 280  $\Omega$  per square, with 80% optical transparency, a high electron mobility of 3700  $\text{cm}^2 \text{V}^{-1} \text{s}^{-1}$  and the half-integer quantum Hall effect at low temperatures, indicating that the quality of graphene grown by CVD is as high as that of mechanically cleaved graphene. Further modifications of this method allow the preparation of predominantly monolayer graphene films with a size of more than 30 inches, which can be further transferred to a polymer film for the fabrication of transparent electrodes [20].

The electronic interaction of graphene with a metal is of both fundamental and technological interest in view of possible device applications. Recent theoretical calculations

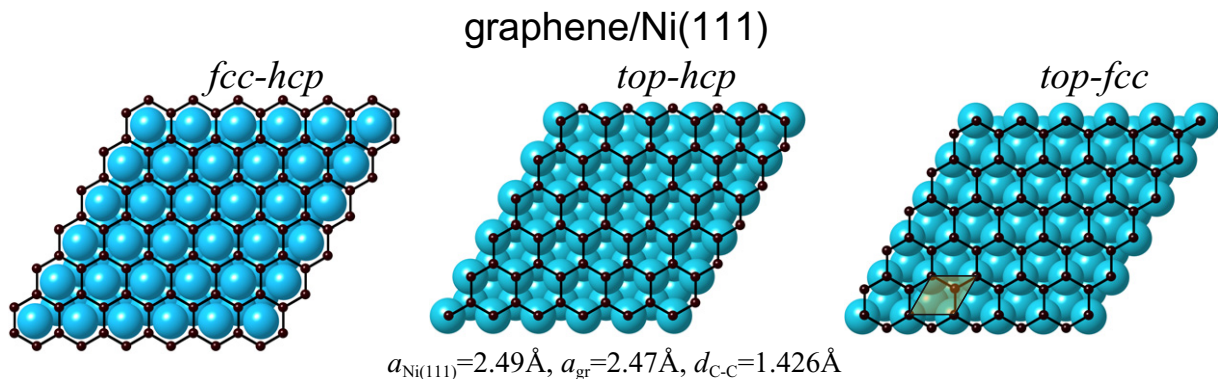


**Figure 1.** Top view of a ball model showing three possible arrangements of the graphene layer on top of the close-packed Ni(111) surface. All structures have threefold symmetry. Left-hand panel: carbon atoms are located above Ni atoms in the 2nd and 3rd Ni layer—hcp-fcc structure; middle panel: carbon atoms are above Ni atoms in the 1st and 2nd layers—top-hcp structure; right-hand panel: carbon atoms are placed above Ni atoms in the 1st and 3rd layers—top-fcc structure. Carbon atoms are small black spheres; the first, second and third layer of Ni atoms are large blue spheres.

by Karpan *et al* [21, 22] for graphene/metal interfaces imply the possibility of an ideal spin filtering in the current-perpendicular-to-the-plane configuration (CPP) for the ferromagnet/graphene/ferromagnet sandwich-like structures. The close-packed surfaces of Co and Ni were considered as ferromagnetic (FM) electrodes, which perfectly coincide with graphene from the crystallographic point of view (figure 1). The spin-filtering effect originates from the unique overlap of the electronic structures of the graphene monolayer and close-packed surfaces of FM Ni and Co. As discussed earlier, graphene is a semimetal with electronic density in the vicinity of  $E_F$  at the corners ( $K$  points) of the hexagonal Brillouin zone of graphene (figure 2). If the Fermi surface projections of the FM metals, fcc Ni or Co, on the (111) close-packed plane are considered, then in both cases graphene has only minority electron density around the  $K$  points of the surface Brillouin zone. In this case, it is expected that in the absence of any additional factors that lower the symmetry of the system, the preferential transport of only minority electrons and perfect spin-filtering will appear in an FM/graphene/FM stack [21, 22]. The interaction between graphene and FM material will, however, change the electronic properties of the interface, partially quenching the spin-filtering effect in the sandwich-like structure, but a sizable effect can still be detected by choosing the proper combination of FM materials [23], and this effect is predicted to increase strongly when multilayer graphene is used [21, 22].

Besides spin filtering, graphene might be the best material for the realization of spintronic devices. Such systems usually require the effective injection of the spin-polarized electrons in the conductive channel, which can be made from graphene [24]. However, prior to being able to implement graphene/ferromagnet systems in any kind of spintronic unit, a study of the electronic, magnetic and interfacial properties has to be performed.

In the present paper, the crystallographic structure, morphology, electronic and magnetic properties of a graphene/ferromagnet interface are considered for the case of the Ni(111)

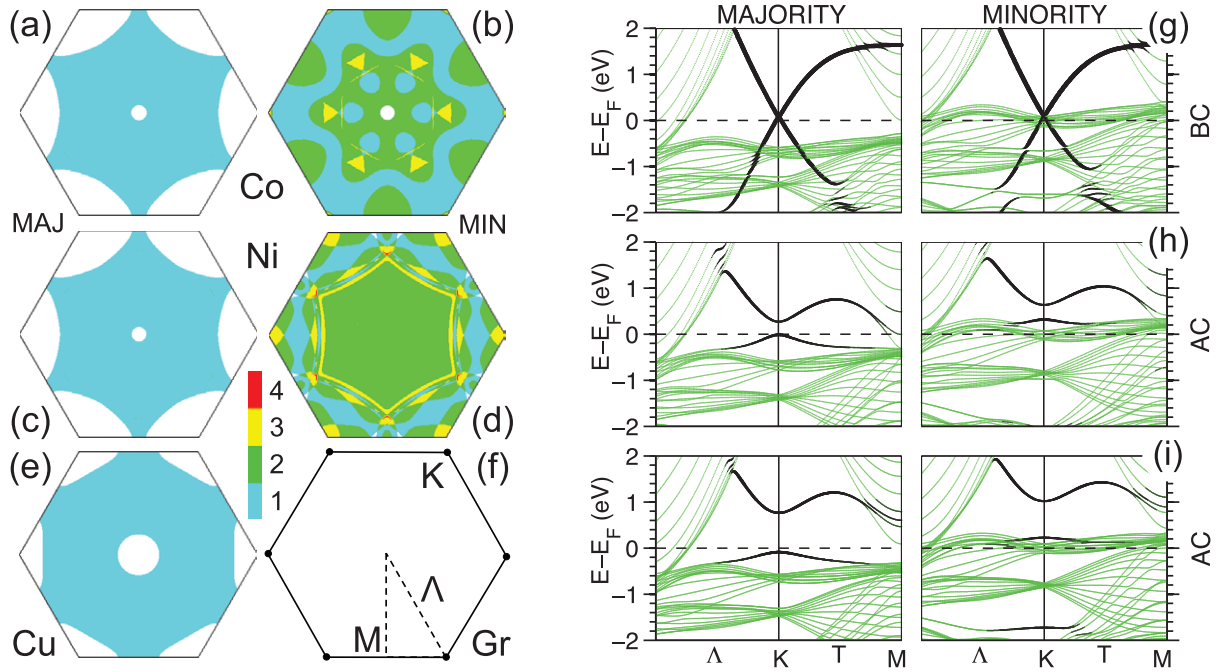


**Figure 2.** Left-hand panel: Fermi surface projections onto the (111) close-packed plane for (a, b) fcc Co (majority and minority spins), (c, d) fcc Ni (majority and minority spins) and (e) fcc Cu. For graphene (f), the constant-energy surface is centered at the  $K$  point of the 2D interface Brillouin zone. Right-hand panel: the results of band structure calculations (majority and minority spins) for (g) fcc-hcp (BC) and (h, i) top-fcc (AC) configurations of carbon atoms on Ni(111). The weight of the carbon  $p_z$  character is shown by black lines where its thickness reflects the corresponding orbital weight. Reprinted with permission of Karpan *et al* [22]. Copyright 2008 by the American Physical Society.

close-packed surface. Scanning tunneling microscopy (STM) investigation shows that perfectly ordered epitaxial graphene layers can be prepared on Ni(111). X-ray absorption spectroscopy (XAS) studies of graphene/Ni(111) reveal the existence of interface states, which originate from the strong hybridization of the graphene  $\pi$  and Ni 3d valence-band states with the partial charge transfer of the spin-polarized electrons onto the graphene  $\pi^*$  unoccupied states. We employ both x-ray magnetic circular dichroism (XMCD) and spin-resolved photoemission (PES) to show that an induced magnetic on carbon atoms appears at the graphene/Ni(111) interface. Further on, angle-resolved photoemission (ARPES) is used to study the modification of the valence-band states of Ni and graphene due to hybridization. By the 3D mapping of electronic states, detailed information about the band structure of the graphene/Ni(111) system is obtained. Analysis of the Fermi surface of the graphene/Ni(111) system indicates very good agreement between experimental and calculated 2D pictures of electronic states in the valence band.

## 2. Experimental details

The present studies of the graphene/Ni(111) interface were performed in different experimental stations in identical experimental conditions, allowing for reproducible sample quality in

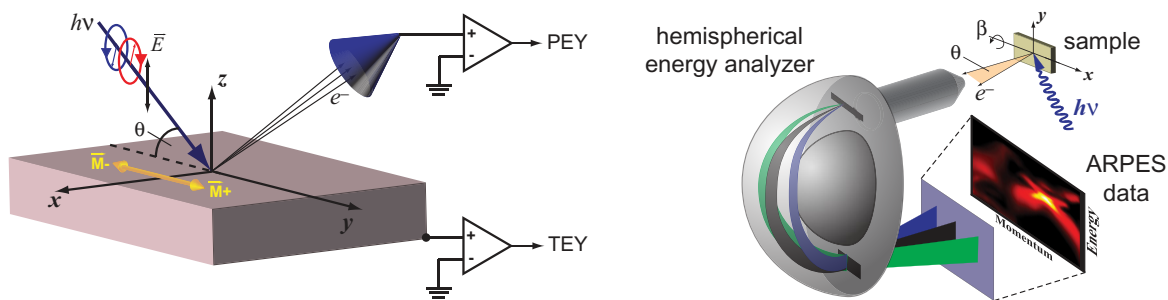


**Figure 3.** Schematic representation of the experimental spectroscopic methods: XAS and XMCD (left) and angle-resolved photoelectron spectroscopy (right). In XAS or XMCD experiments, the photon energy of incoming linearly or circularly polarized light, respectively, is tuned over a particular absorption edge and total or partial electron yield is measured. XMCD spectra are collected in the remanent magnetic state of the sample. In ARPES measurements, the light of a fixed photon energy ( $h\nu$ ) and polarization is used and electrons are analyzed by their kinetic energy,  $E_{\text{kin}}$ , and emission angle,  $\theta$ , and detected by a 2D CCD detector allowing measurement of the sample electronic structure along the  $k_x$  direction in one shot. Rotation of the sample by angle  $\beta$  produces 3D data sets of experimental photoemission intensity,  $I(E_{\text{kin}}, k_x, k_y)$ , where  $k_y$  is the second in-plane component of the wave vector calculated from the experimental geometry.

different experiments. In all experiments, the W(110) single crystal was used as a substrate. Prior to preparation of the graphene/Ni(111) system, the well-established cleaning procedure of the tungsten substrate was applied: several cycles of oxygen treatment with subsequent flashes to 2300 °C. A well-ordered Ni(111) surface was prepared by thermal deposition of Ni films with a thickness of more than 200 Å on to a clean W(110) substrate and subsequent annealing at 300 °C. An ordered graphene overlayer was prepared via thermal decomposition of propene ( $\text{C}_3\text{H}_6$ ) according to the recipe described elsewhere [8, 9], [25]–[27]. The quality, homogeneity and cleanliness of the prepared graphene/Ni(111) system were verified by means of low-energy electron diffraction (LEED), STM and both core-level and valence-band photoemissions.

STM experiments were carried out in an ultra-high vacuum (UHV) system (base pressure  $8 \times 10^{-11}$  mbar) equipped with an Omicron variable temperature scanning tunneling microscope. All STM measurements were performed in the constant-current mode at room temperature using electrochemically etched polycrystalline tungsten tips cleaned in UHV by flash annealing. The sign of the bias voltage corresponds to the voltage at the sample. Tunneling parameters are given separately for each STM image:  $U_T$  for tunneling voltage and  $I_T$  for tunneling current.

XAS and XMCD spectra were collected at the D1011 beamline of the MAX-lab Synchrotron Facility (Lund, Sweden) at both Ni  $L_{2,3}$  and C  $K$  absorption edges in the partial (repulsive potential  $U = -100$  V) and total electron yield modes (PEY and TEY, respectively) with an energy resolution of 80 meV. The left-hand panel of figure 3 shows a schematic representation of the experimental geometry. Magnetic dichroism spectra were obtained with circularly polarized light (the degree of polarization is  $P = 0.75$ ) at different angles  $\theta$  in the remanence magnetic state of the graphene/Ni(111) system after applying an external magnetic



field of 500 Oe along the  $\langle 1\bar{1}0 \rangle$  easy magnetization axis of the Ni(111) film. All absorption measurements were performed at 300 K. The base pressure during the measurements did not exceed  $1 \times 10^{-10}$  mbar.

ARPES experiments were performed at the UE56/2-PGM-1 beam line at BESSY (Berlin, Germany). The experimental station consists of two chambers: preparation and analysis. The sample preparation procedure (oxygen treatments and flashing of W(110) as well as the preparation of the graphene/Ni(111) system) was performed in the preparation chamber after which the sample was transferred to the analysis chamber for further photoemission measurements. The photoemission intensity data sets  $I(E, k_x, k_y)$  were collected with a PHOIBOS 100 energy analyzer (SPECS), while the graphene/Ni(111)/W(110) sample was placed on a six-axis manipulator (three translation and three rotation axes) (figure 3, right-hand panel). The temperature of the sample during the measurements was kept at 80 or 300 K. The energy/angular resolution was set as 80 meV/0.2°. In the case of the spin-resolved PES experiments, the mini-Mott-spin detector (SPECS) was used instead of the 2D CCD detector. The spin-resolved spectra were collected in the remanent magnetic state of the graphene/Ni(111) system (see above) in normal emission geometry. The effective Sherman function was estimated to be  $S_{\text{eff}} = 0.1$  and the instrumental asymmetry was accounted for by measuring the spin-resolved spectra for two opposite directions of the sample magnetization. The base pressure during all photoemission measurements was below  $7 \times 10^{-11}$  mbar.

### 3. Results and discussion

#### 3.1. Growth and surface structure of graphene on Ni(111)

In order to check the quality of the samples directly after each preparation step as well as to provide structural details of the graphene sheets at the atomic level, we performed *in situ* STM measurements at room temperature. Figure 4(a) shows an STM image of the clean atomically flat W(110) surface. The  $(1 \times 1)$  LEED pattern of twofold symmetry (inset of figure 4(a)), typical of the bcc W(110) surface, confirms its high quality. The surface morphology of a 200 Å-thick Ni(111) film deposited on W(110) is shown in figure 4(b). Atomically flat terraces separated by steps are visible in the STM image, which give clear evidence of the epitaxial growth of Ni(111). After the Ni deposition a well-ordered hexagonal  $(1 \times 1)$  LEED pattern was observed (inset of figure 4(b)). Since Ni(111) and graphene have nearly similar lattice parameters (the lattice mismatch is only 1.3%), graphene forms the hexagonal  $(1 \times 1)$  structure. Figure 4(c) shows an overview of a graphene domain on Ni(111) after thermal decomposition of propene. The graphene layer is continuous and exhibits a highly ordered crystallographic structure without any visible defects even over large areas. Figure 4(d) presents a magnified topographic image of the graphene lattice together with a typical LEED pattern of monolayer graphene on Ni(111) (inset of figure 4(d)). A higher-magnification STM image of the graphene surface is shown in figure 4(e) with the graphene hexagonal atomic arrangement marked in the image.

So far, several possible atomic configurations have been considered for the graphene/Ni(111) interface. The three ‘high-symmetry’ structures are known as hcp-fcc, top-hcp, and top-fcc and they are shown in figures 1(a)–(c), respectively. In the top-hcp configuration, the C atoms are placed directly above the Ni atoms of the first layer (top site) and the second layer (hcp site). In top-fcc, the C atoms are arranged above the Ni atoms of

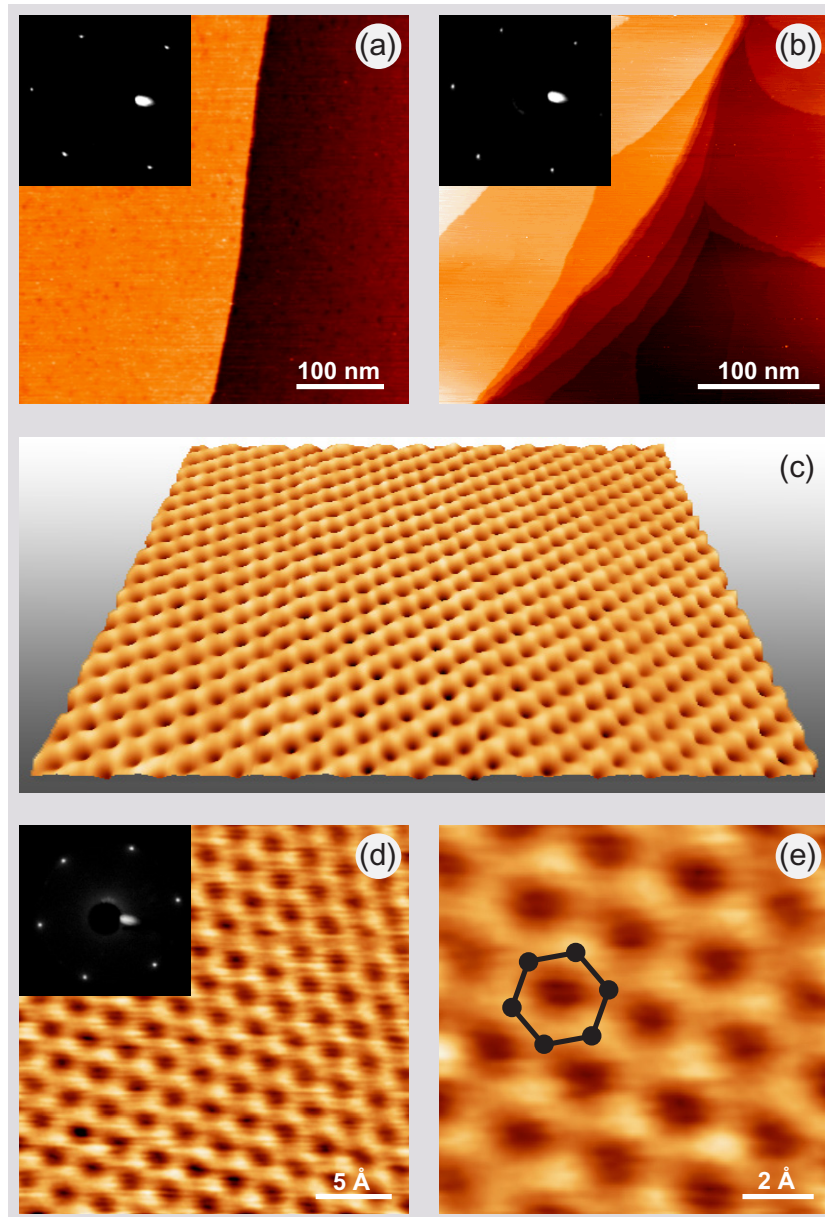


**Figure 4.** (a) Large-scale STM image of the W(110) surface showing atomically flat terraces. Tunneling parameters:  $U_T = 0.8$  V and  $I_T = 11$  nA. Inset: a LEED image of the W(110) surface taken at a primary electron energy of 69 eV. (b) Large-scale STM image of the epitaxial Ni(111) layer grown on the W(110) substrate. Tunneling parameters:  $U_T = 0.5$  V and  $I_T = 0.7$  nA. Inset: a LEED image of the Ni(111) surface taken at a primary electron energy of 67 eV. (c–e) The high-quality graphene/Ni(111) system. (c) Large-scale constant current STM image of the graphene/Ni(111) surface. Tunneling parameters:  $U = 0.002$  V and  $I = 48$  nA. (d) Magnified STM image of the perfect graphene lattice. The inset shows a LEED image obtained at 63 eV. (e) High-magnification STM image showing the atomic structure of the graphene monolayer. Tunneling parameters:  $U_T = 0.002$  V and  $I = 48$  nA. The graphene hexagonal atomic arrangement is marked in (e).

the first and third (fcc) layers. In the hcp-fcc configuration, the C atoms are placed above the hcp and fcc sites. Three additional configurations were considered recently, which were called bridge-top, bridge-fcc and bridge-hcp. In these structures, the C atoms are not placed in hcp-fcc, top-hcp and top-fcc sites but in between [28].

At the moment, no clear consensus exists about which of the above described structures is more energetically stable and which kind of structures are observed in experiments. From the theoretical side, Bertoni *et al* [29] used density functional theory (DFT) with the Perdew, Burke and Ernzerhof generalized gradient approximation (GGA-PBE), which yielded the top-fcc as the most stable atomic configuration at the graphene/Ni(111) interface. DFT-PBE studies were also performed by Kalibaeva *et al* [30], reporting that the top-fcc structure is the lowest energy configuration, whereas hcp-fcc is shown to be unstable. The calculations including three additional ‘low symmetry’ configurations showed that within DFT with GGA-PBE, none of the structures are stable at the experimentally relevant temperatures; with local-density approximation (LDA), the bridge-top configuration was found to be the most energetically favorable one [28]. From the experimental side, Rosei *et al* [31] and Klink *et al* [32] found that the most stable structure is hcp-fcc, whereas Gamo *et al* [7] found top-fcc to be the most favorable configuration.

In our case, graphene terraces have a peak-to-peak roughness of  $0.2 \text{ \AA}$  and show a honeycomb structure with a lattice constant of  $2.4 \pm 0.1 \text{ \AA}$  (figure 4(d)), which agrees well with the expected  $2.46 \text{ \AA}$  lattice spacing of graphene. STM images show that in the honeycomb unit cell, carbon atoms corresponding to different sites appear with a different contrast, which can be attributed to the differences in the local stacking of the graphene sheet and the Ni(111) substrate. Therefore, we interpret our STM images in the following way: figure 4 shows single-layer graphene, where carbon atoms most possibly occupy positions corresponding to one of the two non-equivalent configurations—top-fcc or top-hcp. However, it proves to be impossible to directly identify which of the sites are occupied.

Additionally, different orientations of the graphene relative to the Ni(111) substrate could be observed. Figure 5 shows a moiré structure, indicating a slight rotation of the graphene layer relative to the Ni(111) substrate, demonstrating the simultaneous existence of different stackings in the graphene/Ni(111) system. Two regions showing different apparent heights can be distinguished on the surface (see figure 5). This observation shows that although the interaction between nickel and graphene is relatively strong, different adsorption geometries are locally possible. We would like to note that such areas represent a very rare case compared with the normal graphene structure, as supported by STM, LEED and photoemission measurements.

### 3.2. Bonding and magnetism at the graphene/Ni(111) interface

In order to address the average spatial orientation of selected molecular orbitals (for example  $\pi$  or  $\sigma$ ) at the graphene/Ni interface, we vary the sample orientation with respect to the wave vector of the linearly polarized x-ray light and monitor the absorption intensity. The observed changes of the XAS lineshape at the C *K* edge in the graphene/Ni(111) system represent a nice example demonstrating the so-called *search-light-like* effect [33], which in general can be used for probing the quadrupole moment of the local charge around the absorbing atom. In such an experiment, the absorption intensity associated with a specific molecular orbital final state has a maximum if the electric field vector is aligned parallel to the direction of maximum charge or hole density, i.e. along a molecular orbital, and the intensity vanishes if the electric field vector



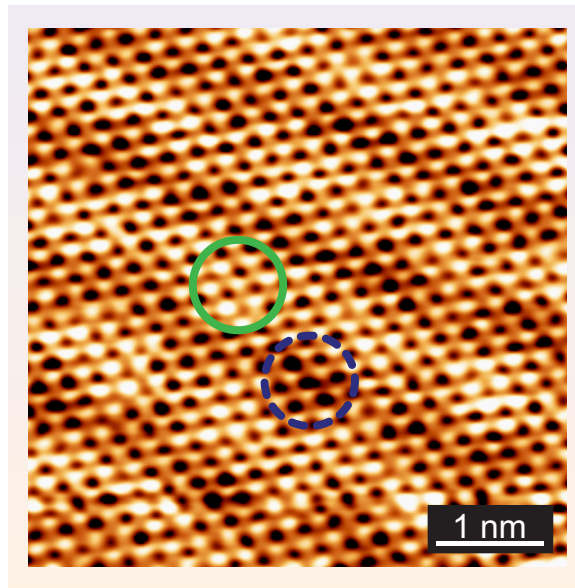


**Figure 5.** Graphene lattice slightly rotated relative to the Ni(111) substrate, showing a moiré structure. Areas of different apparent heights are marked in the image by circles. Tunneling parameters:  $U_T = 1.1$  V and  $I_T = 0.18$  nA.

is perpendicular to the orbital axis. A detailed description of the angular dependence of XAS intensities can be found elsewhere [33, 34].

Figure 6(a) shows XAS spectra of the graphene/Ni(111) system recorded at the C  $K$  absorption edge as a function of the angle  $\theta$  between the direction of the incident linearly polarized x-ray light and the sample surface, e.g. between the electrical field vector of light and the sample surface normal (see the inset of figure 6 for the exact geometry of the experiment). The reference XAS spectrum of the graphite single crystal measured at  $\theta = 30^\circ$  is shown in the upper part of the figure. The spectral features in the two broad regions 283–289 eV and 289–295 eV can be ascribed to C  $1s \rightarrow \pi^*$  and C  $1s \rightarrow \sigma^*$  transitions of core electrons into unoccupied states ( $\pi^*$ ,  $\sigma_1^*$  and  $\sigma_2^*$ ), respectively. The XAS lineshape in both regions is influenced by considerable excitonic effects—poor core-hole screening [36]–[38]. On the comparison of the XAS C  $1s \rightarrow \pi^*$ ,  $\sigma^*$  spectrum of the graphene/Ni(111) system with the reference graphite spectrum, considerable changes in the spectral shapes are observed, which can be attributed to a strong chemisorption. A broadening of the  $\pi^*$  and  $\sigma^*$  resonances gives evidence for a strong orbital hybridization and electron sharing at the graphene/Ni interface, indicating a strong delocalization of the corresponding core-excited state. A comparison of the present XAS results for graphene on Ni(111) with those recently obtained for graphene/Rh and graphene/Ru [39] indicates the existence of a very strong covalent interfacial bonding between carbon atoms in the graphene layer and Ni atoms of the substrate.

Both the atomic and the electronic structure of the graphene/Ni(111) system have recently been calculated by Bertoni *et al* [29]. The calculation yielded the top-fcc configuration of carbon atoms (see figure 1 and the previous section for details) to be energetically the most favorable one and gave a clear indication of the strong interaction between the graphene layer and the substrate. Similar results were obtained for graphene/Co(0001) [40]. This interaction manifests itself by a considerable modification of the graphene- and Ni-related valence-band states as a result of the hybridization of the graphene  $\pi$  and the Ni 3d states accompanied

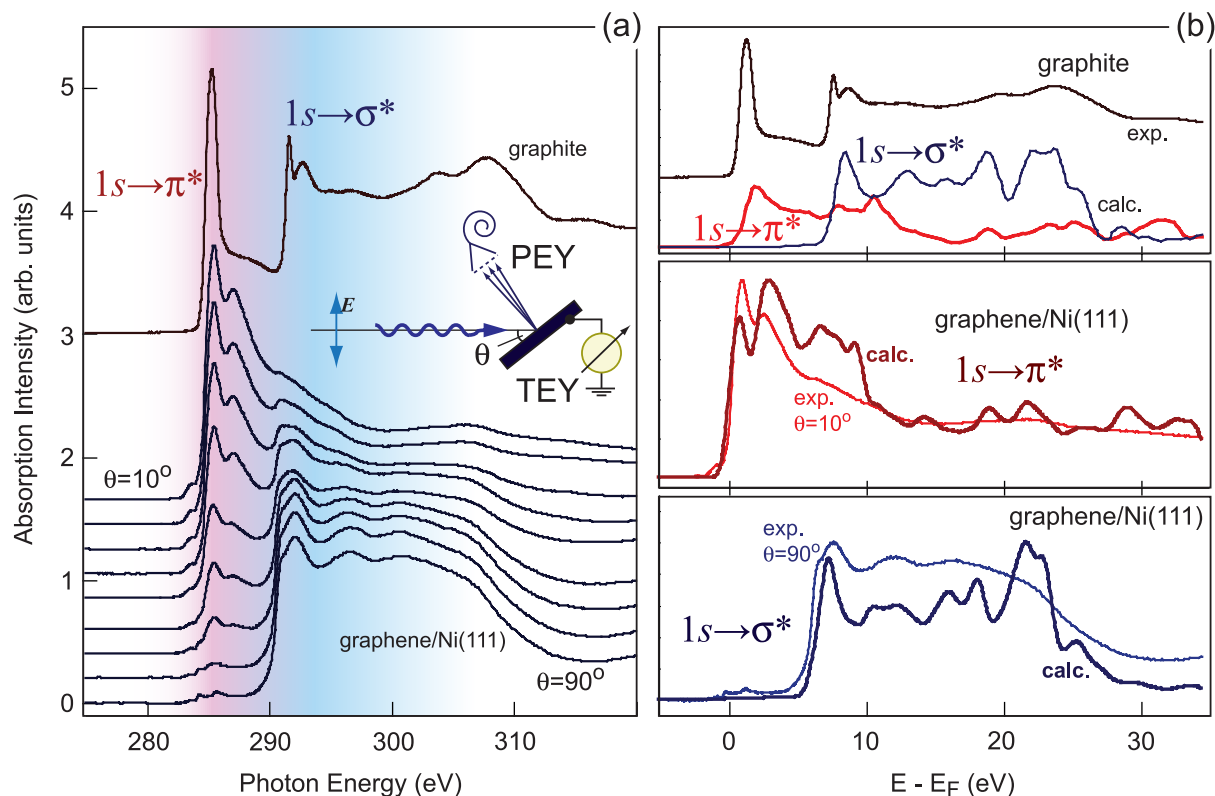


**Figure 6.** (a) Polarization dependence of the absorption at the C  $K$  edge of the graphene/Ni(111) system measured as a function of the angle  $\theta$  (see figure 3, left panel) between the polarization vector of incoming linearly polarized light and the surface normal of the sample [35]. Spectra were collected in the partial electron yield mode and the angle was changed with a step of  $10^\circ$  from the top to the bottom. The reference spectrum of a pure graphite single crystal is shown in the upper part of the panel for comparison. (b) Comparison between experimental XAS spectra and calculated EELS spectra of graphite and graphene/Ni(111) for two different incident angles  $\theta$  where transitions from the C  $1s$  core level on mostly  $\pi^*$ - or  $\sigma^*$ -states occurred. The theoretically calculated spectra have been reproduced with permission of Bertoni *et al* [29]. Copyright 2004 by the American Physical Society.

by a partial charge transfer of spin-polarized electrons from the FM substrate to graphene. These calculations also predict that several occupied and unoccupied interface states ( $I_1$ – $I_5$ ) are formed in this system, which lead to noticeable modifications of the carbon  $K$  edge electron loss spectroscopy (EELS) spectrum. A detailed description of the electronic structure of the graphene/Ni(111) system including the interface states will be given in the next section in conjunction with a discussion of the ARPES results.

In the following, we would like to compare our XAS results with the recently calculated C  $K$  edge EELS spectra for the graphene/Ni(111) interface [29]. In this case, experimental XAS spectra taken at  $\theta = 10^\circ$  and  $\theta = 90^\circ$  correspond to the calculated EELS spectra for the scattering vector  $\mathbf{q}$  perpendicular and parallel to the graphene layer, respectively. The calculated

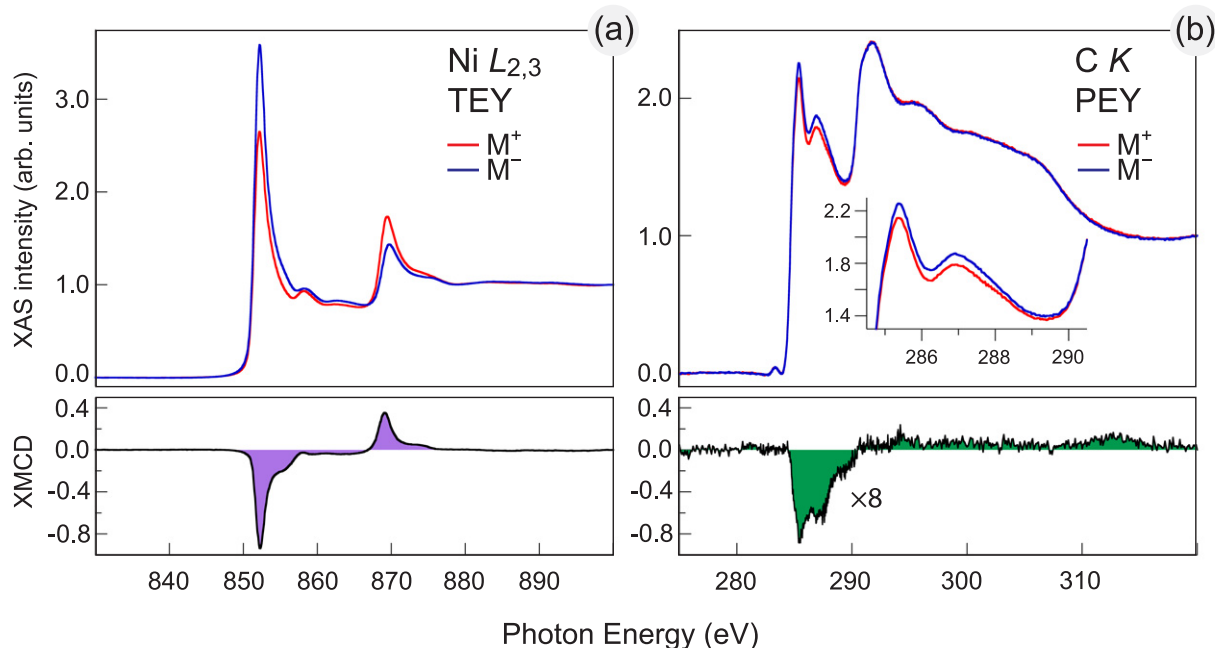


**Figure 7.** XMCD spectra of the graphene/Ni(111) system [35]: absorption spectra measured with circularly polarized light for two opposite orientations of the sample magnetization are shown in the upper part for the Ni  $L_{2,3}$  (a) and C  $K$  edges (b). The corresponding differences reflecting the strength of the dichroic signal are shown in the lower part of the respective figures.

EELS spectra are found to agree well with the experimental XAS data (see figure 6(b)): (i) the spectra show the same angle (scattering vector) dependence and (ii) the experimentally observed XAS features are well reproduced in the calculated EELS spectra. For example, two peaks in the XAS spectra in the  $1s \rightarrow \pi^*$  spectral region at 285.5 and 287.1 eV photon energy can be assigned to the double-peak structure in the calculated EELS spectrum at 0.8 and 3.0 eV above the Fermi level [29]. According to the theoretical calculations [29], the first sharp feature in the XAS spectrum is due to the transition of the electron from the  $1s$  core level to the interface state  $I_4$  above the Fermi level (around the  $K$  point in the hexagonal Brillouin zone), which originates from the  $C p_z$ -Ni  $3d$  hybridization and corresponds to the antibonding orbital between a carbon atom C-top and an interface Ni atom. The second peak in the XAS spectrum is due to the dipole transition of an electron from the  $1s$  core level to the interface state  $I_5$  above the Fermi level (around the  $M$  point in the hexagonal Brillouin zone), which originates from  $C p_z$ -Ni  $p_x, p_y, 3d$  hybridization and corresponds to a bonding orbital between C-top and C-fcc atoms, involving an Ni interface atom. The small feature at 283.7 eV and the low-energy shoulder in the  $1s \rightarrow \pi^*$  absorption spectra probably partly originate from the interface state  $I_4$ , which is located very close to the Fermi level. In the case of the XAS  $C 1s \rightarrow \sigma^*$ , the theory also correctly describes the shape of the absorption spectra [29].

The strong hybridization between graphene  $\pi$  and Ni  $3d$  valence-band states at the graphene/Ni(111) interface leads to the partial charge transfer of the spin-polarized electrons from Ni to C atoms with the appearance of an induced effective magnetic moment of carbon atoms [29], which can be detected in an experiment that is sensitive to the magnetic state of particular elements, like XMCD. Figure 7 shows XAS spectra of the graphene/Ni(111)

system obtained for two opposite magnetization directions with respect to the polarization of the incident x-ray beam (upper panels) together with the resulting XMCD signal (lower panels). The spectra collected at the Ni  $L_{2,3}$  edge in TEY mode and at the C  $K$  edge in PEY mode are presented in the left-hand panel and the right-hand panel, respectively. The Ni  $L_{2,3}$  XMCD spectrum (white line as well as fine structure behind the absorption edge) is in perfect agreement with previously published spectroscopic data [41]–[43]. The quantitative analysis of the absorption spectra obtained on a magnetic sample with circularly polarized light can be performed with the help of the so-called sum rules for spin and orbital magnetic moments [44, 45]. The intensities of  $L_3$  and  $L_2$  absorption lines and their differences for the parallel and anti-parallel orientations of the projection of photon spin on the sample magnetization direction are quantitatively related by the sum rules to the number of 3d holes in the valence band of the FM material and the size of the spin and orbital magnetic moments.

From the experimental Ni  $L_{2,3}$  TEY XAS data (figure 7), the bulk values of Ni magnetic moments were derived, using a number of 3d holes in the valence band of Ni  $n_h = 1.45$  [47] and polarization of light  $P = 0.75$ . At room temperature and in TEY mode (more bulk sensitive), Ni provides a spin moment of  $\mu_S = 0.69\mu_B$  and an orbital moment of  $\mu_L = 0.07\mu_B$ , respectively. These values coincide with the previously published experimental results [41, 48]. The experimentally obtained spin magnetic moment is very close to the calculated bulk value of  $\mu_S = 0.67\mu_B$  for the graphene/Ni(111) system [29]. For the most energetically favorable configuration of carbon atoms on Ni(111), top-fcc, the calculations predict a reduction of the spin magnetic moments of Ni interface atoms by 16 % down to  $0.56\mu_B$  [29]. The experimental data collected at the Ni  $L_{2,3}$  absorption edge in the PEY mode (more surface/interface sensitive) also show a slight reduction of the spin moment to  $\mu_S = 0.63\mu_B$ . However, the observed decrease is not as pronounced as that yielded by the theoretical calculation, which can be explained by the large contribution of the bulk-derived signal to the XMCD spectra.

The most important and interesting result of these XMCD experiments on the graphene/Ni(111) system is the observation of a relatively large dichroic contrast at the C  $K$  absorption edge (figure 7(b)). In order to magnify the measured magnetic contrast at the  $1s \rightarrow \pi^*$  absorption edge, these XMCD spectra were collected in the PEY mode with the circularly polarized light at an angle of  $\theta = 20^\circ$ . We note that the observed differences in the XAS spectra collected at this angle, visible in figures 6 and 7, are due to the different polarization of light: in figure 6(a), the data are obtained with the linearly polarized x-rays, i.e. the strong angular dependence of the absorption signal is due to the different graphene orbital orientations, whereas the data in figure 7 are obtained with the circularly polarized light, i.e. both  $1s \rightarrow \pi^*$  and  $1s \rightarrow \sigma^*$  transitions are nearly equivalently possible. The C  $K$  XMCD spectrum shows that the major magnetic response stems from transitions of the  $1s$  electron to the  $\pi^*$ -states, while transitions to the  $\sigma^*$ -states yield a very weak (if any) magnetic signal. These results indicate that only the C  $2p_z$  orbitals of the graphene layer are magnetically polarized due to the hybridization with the Ni 3d band. The sharp structure at the  $1s \rightarrow \pi^*$  absorption edge originates from hybridized C  $p_z$ -Ni 3d and C  $p_z$ -Ni  $p_x, p_y$  3d states (see earlier discussion and [29]).

The appearance of XMCD signal at the C  $K$  edge shows that indeed the Ni film induces a magnetic moment in the graphene overlayer. However, at the C  $K$  absorption edge, the electron transitions occur from the non-spin-orbit split  $1s$  initial states to the  $2p$  final states and, thus, in the analysis of the dichroism effect at the  $K$  edge, one equation in the selection rules is missed. This means that the XMCD signal at  $K$  edges provides information only on the orbital magnetic



moment  $\mu_{\text{orb}}$  [44]–[46]. The partial charge transfer from Ni to C atoms in the graphene/Ni(111) system was calculated for the 22-atom (graphene)/Ni cluster [49], yielding  $0.205e^-$  per C atom in graphene, which leads to the 2p-orbital occupation number of  $n_p = 2.205e^-$ . Using the C *K* XAS spectra and applying the procedure described in the work [46], an orbital moment of  $\mu_{\text{orb}} = 1.8 \pm 0.6 \times 10^{-3} \mu_B$  per C atom was extracted. The relatively large uncertainty arises mainly from the estimation of the number of C 2p holes, the background subtraction of XAS spectra, and from the error for the degree of circular polarization of light.

The theoretical work [29] also gives the values for spin magnetic moment of  $-0.01\mu_B$  and  $0.02\mu_B$  for C-top and C-fcc atoms, respectively. However, the magnetic splitting of the majority and minority parts of the interface states  $I_3$  and  $I_4$  was found to be between 0.13 and 0.55 eV, respectively, which may yield higher values for the magnetic moment. Due to the impossibility to directly extract the value of the spin magnetic moment from the *K* edge XMCD spectra, we apply a simple comparison with the magnetic measurements on similar systems in order to estimate the average  $\mu_S$  value for the carbon atoms at the graphene/Ni(111) interface. For the Fe/C multilayers, clear magnetic signals of carbon were obtained by using the resonant magnetic reflectivity technique [50]. The hysteresis loop recorded at the C *K* absorption edge gave a clear proof of ferromagnetism of carbon atoms at room temperature with a measured spin magnetic moment of  $\mu_S = 0.05\mu_B$  induced by adjacent Fe atoms. The observed ferromagnetism of carbon in the Fe/C multilayered system was related to the hybridization between the Fe 3d orbitals and the C  $p_z$  orbitals, which are normal to the graphene-type layered  $sp^2$  coordination. The second comparison can be performed with carbon nanotubes on FM Co substrate [51]. Carbon nanotubes were shown to become magnetized when they are in contact with magnetic material. Spin-polarized charge transfer at the interface between a flat ferromagnetic metal substrate and a multiwalled carbon nanotube leads to a spin transfer of about  $0.1\mu_B$  per contact carbon atom. Additionally, a comparison of the XMCD spectra obtained at the C *K* edge in graphene/Ni(111) (the present work) and at the O *K* edge in O/Ni(100) [52] reveals approximately the same magnitude of XMCD signal. For the O/Ni(100) system, where an induced spin magnetic moment of  $0.053\mu_B$  on oxygen atoms was calculated, the theoretically simulated XAS and XMCD spectra agree well with the experimental data. Considering these analogous systems, we estimate the induced magnetic moment for graphene on Ni(111) to be in the range of  $0.05\text{--}0.1\mu_B$  per carbon atom.

The experimentally observed effective magnetic moment of carbon atoms of the graphene layer on Ni(111) is also confirmed by our spin-resolved PES results. Figure 8 shows the spin-resolved valence-band spectra (a) and the corresponding spin polarization as a function of the binding energy (BE) (b) of pure Ni(111) and the graphene/Ni(111) system. These spectra were recorded with the photon energy of  $h\nu = 65$  eV at room temperature in normal emission geometry. The spin-resolved PES spectra of the pure thick bulk-like Ni(111) film on W(110) is in very good agreement with previously reported data presenting the clear spin contrast in the valence-band region and a spin polarization value of about  $-60\%$  at the Fermi level. The presence of graphene on Ni(111) strongly modifies the valence-band spectrum of Ni, indicating the strong interaction between valence-band states of graphene and Ni (a thorough discussion of valence-band photoemission spectra will be given in the next section). In the graphene/Ni(111) system, the spin polarization of Ni 3d states at  $E_F$  is strongly reduced to about  $-25\%$ . The considerable modifications of the spin-resolved structure of Ni 3d states as well as the reduction of the spin polarization at  $E_F$  could be considered as an indication of the decrease of magnetic moment of Ni atoms at the graphene/Ni(111) interface. In general, the Ni 3d photoemission

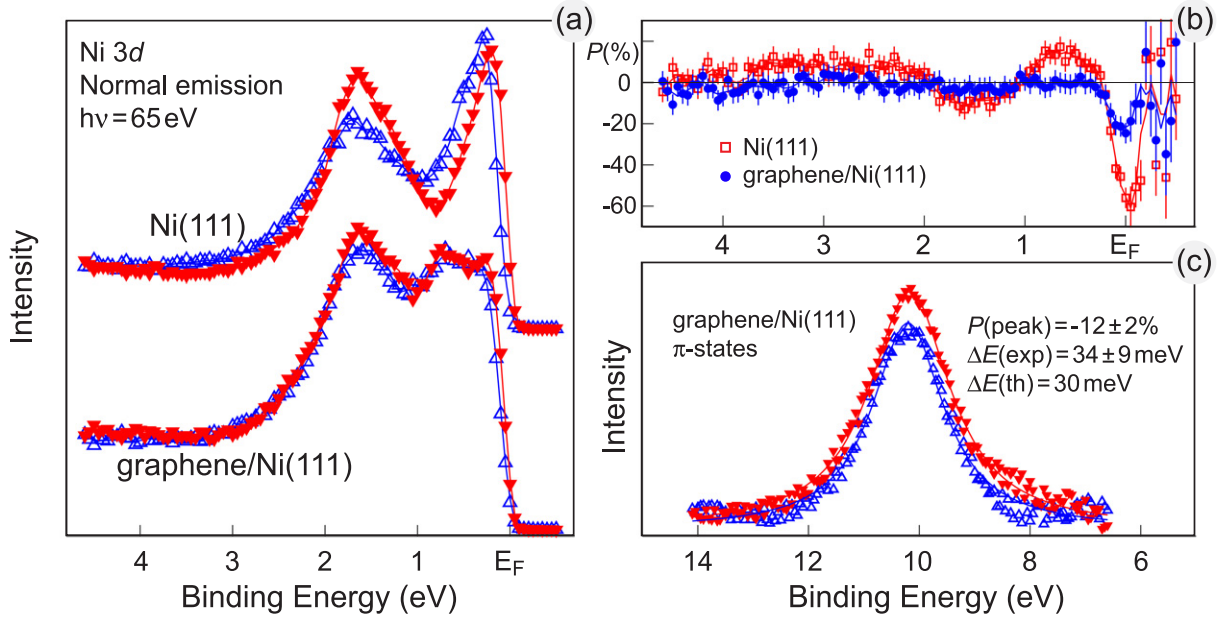


**Figure 8.** (a) Spin-resolved PES spectra and (b) corresponding spin polarization of Ni 3d valence-band states as a function of the BE for Ni(111) and the graphene/Ni(111) system. (c) Spin-resolved PES spectra of the  $\pi$ -states of graphene on Ni(111). A spin polarization value of about  $(-12 \pm 2\%)$  together with a considerable  $\pi$ -band exchange splitting of about 34 meV are observed. All spectra were collected in normal emission geometry with photon energy of 65 eV.

signal around  $E_F$  consists of the sum of the bulk- and surface-derived photoemission intensities. But due to the fact that the presented spectra were collected in the most surface-sensitive regime (the kinetic energy of electrons is  $E_{\text{kin}} \approx 60 \text{ eV}$  and the corresponding inelastic mean free path is  $\lambda \sim 5 \text{ \AA}$ ), the main contribution in these spectra comes from the surface Ni atoms. The same behavior for the surface Ni layer was predicted by theory [29] and was experimentally observed in the presented XMCD measurements.

Figure 8(c) shows the spin-resolved spectra of the  $\pi$ -states of graphene on Ni(111) measured in normal emission geometry with a photon energy of 65 eV. These states are located at 10.1 eV of BE (see the next section for details). After careful subtraction of the background spin polarization that originates from the spin-resolved Ni 3d valence-band states, a clear spin contrast could be detected for the graphene  $\pi$ -states with maximum spin polarization of  $P = -12 \pm 2\%$  at room temperature. The two spin-resolved components are fitted with Lorentzian-shape profiles, giving the exchange splitting of about  $34 \pm 9 \text{ meV}$  for these states, which agrees well with the value extracted from the theoretical work [29]. A comparison of the spin-resolved spectra with the background spin polarization originating from Ni 3d states shows that the spin moment of graphene is aligned antiparallel to the magnetization of Ni, meaning antiparallel magnetic coupling of graphene to Ni. However, this conclusion is based only upon the normal emission spin-resolved measurements and has to be clarified by more detailed spin-resolved PES experiments. Here, we would like to note that experimental evidence of a pronounced spin polarization at room temperature together with the splitting of the  $\pi$  states

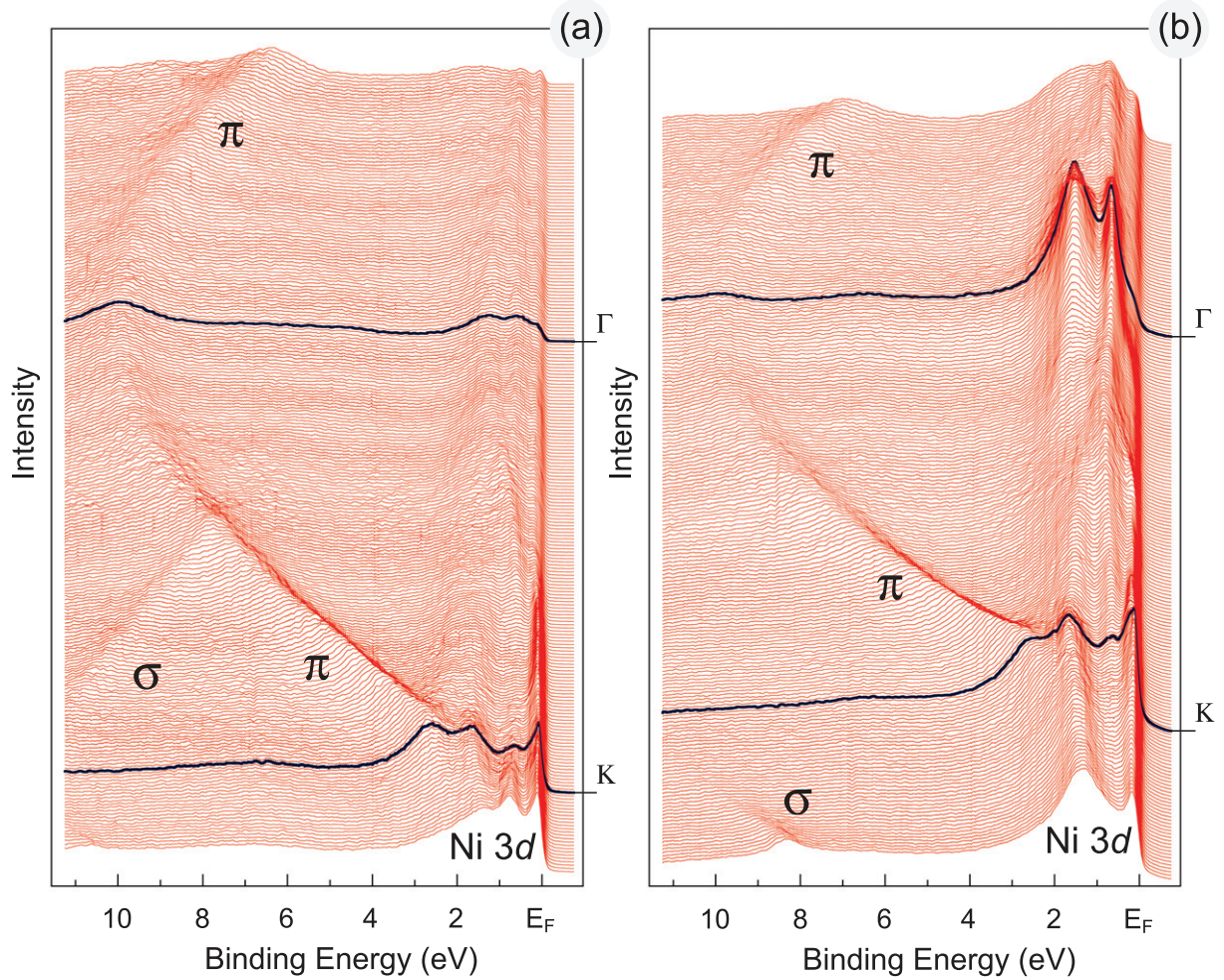


**Figure 9.** ARPES spectra of the graphene/Ni(111) system recorded along the  $\Gamma$ – $K$  direction of the hexagonal Brillouin zone at (a) 70 eV and (b) 100 eV photon energy. Spectra corresponding to  $\Gamma$  and  $K$  points are marked by thick black lines.

in the graphene/Ni(111) system is in contradiction to the results previously reported by Rader *et al* [53], where no or very small spin polarization of the graphene  $\pi$  states was observed. The origin of this discrepancy is, however, not clear at the moment, and further spin-polarized PES investigations of the graphene/Ni(111) system should be undertaken in order to resolve this issue.

### 3.3. Electronic properties of graphene on Ni(111)

Figure 9 shows two series of ARPES spectra measured along the  $\Gamma$ – $K$  direction of the hexagonal Brillouin zone of the graphene/Ni(111) system. Each series is extracted from the 3D sets of data of photoemission intensity  $I(E_B, k_x, k_y)$ , where  $E_B$  is the BE and  $k_x$  and  $k_y$  are the orthogonal components of the in-plane wave vector. For the graphene/Ni(111) system, the  $K$  and  $M$  points of the Brillouin zone are reached at  $1.7$  and  $1.4 \text{ \AA}^{-1}$ , respectively.



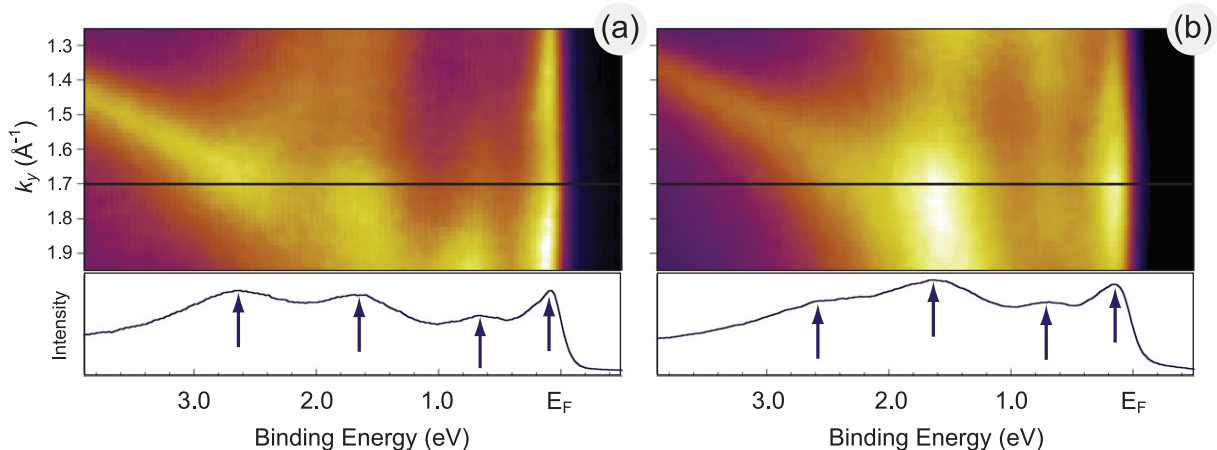


**Figure 10.** Regions around the  $K$  point of photoemission intensity of the graphene/Ni(111) system measured at (a) 70 eV and (b) 100 eV of photon energy. The corresponding intensity profiles at the  $K$  point are shown in the lower panels with arrows indicating the main photoemission features discussed in the text.

Photoemission data presented in figure 9 were collected at two different photon energies: (a) 70 eV and (b) 100 eV. The variation in the photon energy, i.e. photoemission cross-section, gives the possibility to clearly separate the partial contributions of emissions from graphene-derived and Ni-derived valence-band states in the spectra. The presented photoemission data are in very good agreement with previously published results [8, 25, 26, 54, 55], but were acquired with a much better energy/wave-vector resolution allowing for a more accurate analysis of photoemission dispersions. In figure 9, one can clearly discriminate dispersions of graphene  $\pi$ - and  $\sigma$ -derived states in the region below 2 eV BE as well as Ni 3d-derived states near  $E_F$ . The BE of the graphene  $\pi$ -states at the center of the Brillouin zone (at the  $\Gamma$  point) equals 10.1 eV, which is approximately 2.4 eV larger than the BE of these states in pure graphite. The shift to larger BE is different for  $\sigma$  and  $\pi$  valence-band graphene-derived states. This behavior can be explained by the different hybridization strength between these states and Ni 3d valence-band states, which is larger for the out-of-plane-oriented  $\pi$ -states compared with the one for the in-plane-oriented  $\sigma$ -states of the graphene layer. The BE difference of  $\approx 2.4$  eV for the  $\pi$ -states and  $\approx 1$  eV for the  $\sigma$ -states between graphite and graphene on Ni(111) is in good agreement with previously reported experimental and theoretical values [8, 29]. The effect of hybridization between Ni 3d and graphene  $\pi$ -states can be clearly demonstrated in the region around the  $K$  point of the Brillouin zone: (i) one of the Ni 3d bands at 1.50 eV changes its BE by  $\approx 150$  meV to larger BE when approaching the  $K$  point; (ii) a hybridization shoulder is visible in photoemission spectra, which disperses from approximately 1.6 eV to the BE of the graphene  $\pi$ -states at the  $K$  point (see also figure 10 for a detailed view). The strong hybridization observed in PES spectra underlines the fact that the  $\pi$ -states might become spin-polarized and might gain a non-zero magnetic moment due to charge transfer from the Ni atoms to the carbon atoms.

Considering the electronic band structure of the graphene/Ni(111), the region around the  $K$  point delivers the most interesting and important information with respect to the possible spin-filtering effects in the graphene/ferromagnet or ferromagnet/graphene/ferromagnet



**Table 1.** BEs (in eV) of the main valence-band features around the  $K$  point extracted from the calculated band structures of the graphene/Ni(111) system. Positions of experimental photoemission peaks are listed in the right-hand column.

Karpan <i>et al</i> [22]			Bertoni <i>et al</i> [29]			Experiment
Spin $\uparrow$	Spin $\downarrow$		Spin $\uparrow$	Spin $\downarrow$		
0.7	0	Ni 3d	0.8	0	Ni 3d	0.1–0.2
1.2	0.9	Ni 3d	1.5	0.9	Ni 3d	0.7
0.1	–0.2	Ni 3d– gr. $\pi$	2.8	2.1	Ni 3d	1.65
	1.8	Ni 3d– gr. $\pi$	0.2	–0.18	$I_3$	2.65
			2.4	1.96	$I_2$	
			3.37	3.24	$I_1$	

sandwich-like structures. This part of the electronic structure measured with two different photon energies ( $h\nu = 70$  and  $100$  eV) is shown in figure 10 as color maps (upper panels) together with the corresponding intensity profiles directly at the  $K$  point (lower panels). Firstly, the spectral function of the graphene layer on Ni(111) is characterized by the absence of a well-ordered structure of the graphene  $\pi$ -bands in the vicinity of the Fermi level and, secondly, the Dirac cone is not preserved. Both observations can be attributed to a strong interaction between graphene layer and metallic substrate, leading to a strong hybridization between the graphene  $\pi$  and the Ni 3d valence-band states. In the vicinity of the  $K$  point, a number of photoemission peaks can be clearly distinguished: (i) a sharp peak about the Fermi level at 0.1–0.2 eV BE, (ii) a graphene  $\pi$ -states-related peak at 2.65 eV BE and (iii) two peaks at 0.7 and 1.65 eV BEs.

In the following, we perform a detailed analysis of the experimentally obtained electronic structure relying mainly on two comprehensive sets of electronic structure calculations currently available for the graphene/Ni(111) system [22, 29]. The calculations by Bertoni *et al* [29] predict the existence of three interface states below the Fermi level originating from the strong hybridization between the Ni 3d and the graphene  $\pi$ -states and corresponding to ( $I_1$ ) bonding between C-fcc and interface Ni atoms; ( $I_2$ ) bonding between C-top and interface Ni atoms and ( $I_3$ ) antibonding between C-fcc and interface Ni atoms. Karpan *et al* [22] performed band structure calculations of the graphene/Ni(111) system with a major emphasis on the investigation of the spin-dependent transport properties of the Ni/graphene/Ni sandwiches. Both calculations yield quite a complicated band structure of the graphene/Ni(111) system around the Fermi level due to the strong hybridization between the graphene and Ni valence-band states. From an analysis of the region around the  $K$  point of the hexagonal Brillouin zone, we could distinguish a number of flat bands that are clearly separated from each other. The positions of the bands taken from both calculations [22, 29] are summarized in table 1 with the assignment of the particular band character.

The interpretation of the experimentally observed photoemission features around the Fermi level could be performed as presented in the following. The photoemission peak close to the Fermi level (0.1–0.2 eV BE) could be considered as a combination of the interface state  $I_3$  (both spins) with a large contribution of the graphene  $\pi$ -character and the Ni 3d( $\downarrow$ )-band. The second peak at 0.7 eV BE could be assigned to the combination of the Ni 3d( $\uparrow$ )- and Ni 3d( $\downarrow$ )-bands

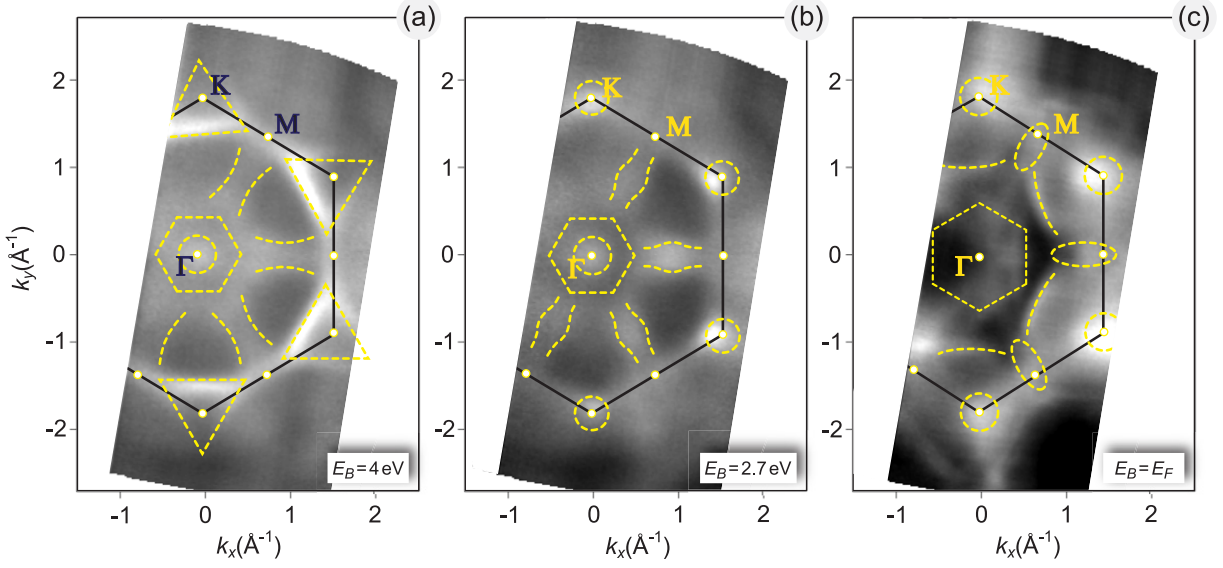


**Figure 11.** Constant energy cuts of the 3D data sets in the energy-wave vector space,  $I(E_B, k_x, k_y)$ , obtained via a  $\beta$ -scan of the graphene/Ni(111) system obtained at 100 meV photon energy. The energy cuts are taken at (a) 4 eV and (b) 2.7 eV BE as well as at (c)  $E_F$ . As supplementary material, we also present a movie (available from [stacks.iop.org/NJP/12/125004/mmedia](http://stacks.iop.org/NJP/12/125004/mmedia)) that shows the BE scan through the valence band of the graphene/Ni(111) system with corresponding energy cuts in the wave vector space. Dashed lines are a guide to the eye.

present in both calculations (the first and second rows in table 1, respectively). The feature at 1.65 eV could be considered as a combination of the Ni 3d( $\uparrow$ )-band and  $I_2(\downarrow)$ -state with a large graphene  $\pi$ -character. The last photoemission peak (2.65 eV BE) could be assigned to the interface state  $I_2(\uparrow)$  with a large contribution of the graphene  $\pi$ -character.

In order to check the theoretical predictions concerning the CPP spin-dependent electronic transport properties of the ideal graphene/Ni(111) interface, we performed a careful analysis of the constant energy photoemission maps close to the Fermi level. We would like to admit that such an analysis can be rather complicated due to the fact that Ni 3d bands, which dominate the photoemission intensity around the Fermi level, are very flat in the vicinity of  $E_F$ . Figure 11 shows the constant energy cuts of the 3D data set obtained at  $h\nu = 100$  eV for the graphene/Ni(111) system. These energy cuts were taken at (a) 4 eV and (b) 2.7 eV BE as well as at (c) the Fermi level. The energy cut at  $E_B = 4$  eV shows characteristic photoemission intensity patterns of the graphene layer, which reflect the symmetry of the system. Below the Dirac point (crossing of straight dispersion lines of  $\pi$ -states in free-standing graphene), the graphene  $\pi$ -bands are visible in the first Brillouin zone, whereas no bands can be seen in the second one. Additionally, several energy bands are present in the middle of the Brillouin zone (outlined by dashed yellow lines), which also show hexagonal symmetry. These bands originate from the hybridization of the Ni and graphene valence-band states. The constant energy cut taken in the region of the minimal BE of the graphene  $\pi$ -states ( $E_B = 2.7$  eV) is shown in figure 11(b). In the case of graphene/Ni(111), the Dirac point is not preserved due to the strong hybridization

of Ni 3d and graphene  $\pi$ -states around the  $K$  point. This can also be directly recognized at this energy cut where graphene  $\pi$ -states produce broad intensity spots instead of sharp points in the wave vector space. As in the previous case, we observe a number of valence-band states in the middle part of the Brillouin zone, which again could be assigned to the hybridization-derived states.

The most interesting and important information in view of the spin-dependent transport properties of the graphene/Ni(111) system can be extracted from the constant energy cut obtained at the Fermi energy, which is presented in figure 11(c). Already the analysis of figures 9(a) and (b) and 10(a) and (b) shows that the photoemission intensity is increased around the  $K$  point and along the  $K$ – $M$  direction of the hexagonal Brillouin zone, which correlates with the increased photoemission intensity observed in the energy cut shown in figure 11(c) for the Fermi energy. Additionally, a number of arcs surrounding the  $K$  points and weak (but distinguished) diamond-shape regions of increased intensity are clearly visible in the middle part and around the  $M$  points of the Brillouin zone, respectively. Upon comparison of the obtained photoemission results for the graphene/Ni(111) system (figures 9–11) with the band structure calculations for this system (figure 2) [21, 22, 29], we observe very good agreement between theory and experiment. In particular, the region around the Fermi level for the ideal graphene/Ni(111) system is well reproduced in the experiment. Unfortunately, at the present stage of the experiment, we cannot specify the spin character of energy bands, which should be the subject of future spin-and angle-resolved photoemission investigations.

#### 4. Conclusions

In conclusion, the structural, magnetic and electronic properties of the high-quality graphene/ferromagnet interface (graphene on Ni(111)) were investigated by means of STM, XAS and XMCD as well as via mapping of the band structure by means of ARPES. The STM investigation showed that perfectly ordered epitaxial graphene layers can be prepared by elevated temperature decomposition of hydrocarbons, with domains larger than the terraces of the underlying Ni(111). A strong modification of the electronic structure of the graphene layer and Ni substrate upon graphene adsorption on the FM substrate was detected by all spectroscopic methods. This modification is due to the considerable hybridization of the graphene  $\pi$  and Ni 3d valence-band states accompanied by the partial charge transfer of spin-polarized electrons from Ni to C atoms, leading to the appearance of the effective magnetic moment in the graphene layer. The presence of an effective magnetic moment on carbon atoms of the graphene layer was unambiguously proven by XMCD and spin-resolved PES measurements. The experimentally obtained electronic structure of occupied and unoccupied states was compared with available band structure calculations allowing the clear assignment of spectral features in the XAS and ARPES data. Good agreement between theory and experiment was also found upon analysis of the Fermi energy cuts, which to some extent supports the theoretically predicted spin-filtering property of the graphene/Ni(111) interface. However, clear assignment of the spectroscopic valence-band features has to be performed in future spin-resolved PES experiments.

#### Acknowledgments

We thank all co-workers and collaborators for their contributions to this work, in particular, K Horn, M Weser, S Böttcher, C Enderlein, A Preobrajenski, E Voloshina, E Goering, M Sicot,

P Leicht and A Zusan. We also thank P Kelly and L Calmels for fruitful discussions. This work was supported by the European Science Foundation (ESF) under the EUROCORES Programme EuroGRAPHENE ('SpinGraph' project). YD acknowledges the financial support of the German Research Foundation (DFG) under project DE1679/2-1. MF acknowledges financial support from the Research Center 'UltraQuantum' (Excellence Initiative), from the Deutsche Forschungsgemeinschaft (DFG) via Collaborative Research Center (SFB) 767 and from the Baden-Württemberg Stiftung.

## References

- [1] Geim A K and Novoselov K S 2007 The rise of graphene *Nat. Mater.* **6** 183
- [2] Castro Neto A, Guinea F, Peres N, Novoselov K and Geim A 2009 The electronic properties of graphene *Rev. Mod. Phys.* **81** 109
- [3] Geim A K 2009 Graphene: status and prospects *Science* **324** 1530
- [4] Novoselov K S, Geim A K, Morozov S V, Jiang D, Katsnelson M I, Grigorieva I V, Dubonos S V and Firsov A A 2005 Two-dimensional gas of massless Dirac fermions in graphene *Nature* **438** 197
- [5] Morozov S V, Novoselov K S, Katsnelson M I, Schedin F, Elias D C, Jaszczak J A and Geim A K 2008 Giant intrinsic carrier mobilities in graphene and its bilayer *Phys. Rev. Lett.* **100** 016602
- [6] Schedin F, Geim A K, Morozov S V, Hill E W, Blake P, Katsnelson M I and Novoselov K S 2007 Detection of individual gas molecules adsorbed on graphene *Nat. Mater.* **6** 652
- [7] Gamo Y Y, Nagashima A, Wakabayashi M, Terai M and Oshima C 1997 Atomic structure of monolayer graphite formed on Ni(111) *Surf. Sci.* **374** 61
- [8] Dedkov Yu S, Fonin M, Rüdiger U and Laubschat C 2008 Rashba effect in the graphene/Ni(111) system *Phys. Rev. Lett.* **100** 107602
- [9] Dedkov Yu S, Fonin M, Rüdiger U and Laubschat C 2008 Graphene-protected iron layer on Ni(111) *Appl. Phys. Lett.* **93** 022509
- [10] Martoccia D *et al* 2008 Graphene on Ru(0001): a  $25 \times 25$  supercell *Phys. Rev. Lett.* **101** 126102
- [11] Sutter P, Hybertsen M S, Sadowski J T and Sutter E 2009 Electronic structure of few-layer epitaxial graphene on Ru(0001) *Nano Lett.* **9** 2654
- [12] Wang B, Bocquet M L, Marchini S, Guenther S and Wintterlin J 2008 Chemical origin of a graphene moiré overlayer on Ru(0001) *Phys. Chem. Chem. Phys.* **10** 3530
- [13] N'Diaye A T, Bleikamp S, Feibelman P and Michely T 2006 Two-dimensional Ir cluster lattice on a graphene moiré on Ir(111) *Phys. Rev. Lett.* **97** 215501
- [14] Coraux J, N'Diaye A T, Busse C and Michely T 2008 Structural coherency of graphene on Ir(111) *Nano Lett.* **8** 565
- [15] Coraux J, N'Diaye A T, Engler M, Busse C, Wall D, Buckanie N, Meyer zu Heringdorf F J, van Gastel R, Poelsema B and Michely T 2009 Growth of graphene on Ir(111) *New J. Phys.* **11** 023006
- [16] Hu Z P, Ogletree D F, Van Hove M A and Somorjai G A 1987 LEED theory for incommensurate overlayers—application to graphite on Pt(111) *Surf. Sci.* **180** 433
- [17] Land T A, Michely T, Behm R J, Hemminger J C and Comsa G 1992 STM investigation of single layer graphite structures produced on Pt(111) by hydrocarbon decomposition *Surf. Sci.* **264** 261
- [18] Sasaki M, Yamada Y, Ogiwara Y, Yagyu S and Yamamoto S 2000 Moiré contrast in the local tunneling barrier height images of monolayer graphite on Pt(111) *Phys. Rev. B* **61** 15653
- [19] Kim K S, Zhao Y, Jang H, Lee S Y, Kim J M, Kim K S, Ahn J H, Kim P, Choi J Y and Hong B H 2009 Large-scale pattern growth of graphene films for stretchable transparent electrodes *Nature* **457** 706
- [20] Bae S *et al* 2010 Roll-to-roll production of 30-inch graphene films for transparent electrodes *Nat. Nanotechnol.* **5** 574
- [21] Karpan V M, Giovannetti G, Khomyakov P A, Talanana M, Starikov A A, Zwierzycki M, van den Brink J, Brocks G and Kelly P J 2007 Graphite and graphene as perfect spin filters *Phys. Rev. Lett.* **99** 176602



- [22] Karpan V M, Khomyakov P A, Starikov A A, Giovannetti G, Zwierzycki M, Talanana M, Brocks G, Van Den Brink J and Kelly P J 2008 Theoretical prediction of perfect spin filtering at interfaces between close-packed surfaces of Ni or Co and graphite or graphene *Phys. Rev. B* **78** 195419
- [23] Yazyev O V and Pasquarello A 2009 Magnetoresistive junctions based on epitaxial graphene and hexagonal boron nitride *Phys. Rev. B* **80** 035408
- [24] Tombros N, Jozsa C, Popinciuc M, Jonkman H T and van Wees B J 2007 Electronic spin transport and spin precession in single graphene layers at room temperature *Nature* **448** 571
- [25] Nagashima A, Tejima N and Oshima C 1994 Electronic states of the pristine and alkali-metal-intercalated monolayer graphite/Ni(111) systems *Phys. Rev. B* **50** 17487
- [26] Dedkov Yu S, Shikin A M, Adamchuk V K, Molodtsov S L, Laubschat C, Bauer A and Kaindl G 2001 Intercalation of copper underneath a monolayer of graphite on Ni(111) *Phys. Rev. B* **64** 035405
- [27] Dedkov Yu S, Fonin M and Laubschat C 2008 A possible source of spin-polarized electrons: the inert graphene/Ni(111) system *Appl. Phys. Lett.* **92** 052506
- [28] Fuentes-Cabrera M, Baskes M I, Melechko A V and Simpson M L 2008 Bridge structure for the graphene/Ni(111) system: a first principles study *Phys. Rev. B* **77** 035405
- [29] Bertoni G, Calmels L, Altibelli A and Serin V 2005 First-principles calculation of the electronic structure and EELS spectra at the graphene/Ni(111) interface *Phys. Rev. B* **71** 075402
- [30] Kalibaeva G, Vuilleumier R, Meloni S, Alavi A, Ciccotti G and Rosei R 2006 *Ab initio* simulation of carbon clustering on an Ni(111) surface: a model of the poisoning of nickel-based catalysts *J. Phys. Chem. B* **110** 3638
- [31] Rosei R, Decrescenzi M, Sette F, Quaresima C, Savoia A and Perfetti P 1983 Structure of graphitic carbon on Ni(111): a surface extended-energy-loss fine-structure study *Phys. Rev. B* **28** 1161
- [32] Klink C, Stensgaard I, Besenbacher F and Lægsgaard E 1995 An STM study of carbon-induced structures on Ni(111): evidence for a carbide-phase clock reconstruction *Surf. Sci.* **342** 250
- [33] Stöhr J and Samant M G 1999 Liquid crystal alignment by rubbed polymer surfaces: a microscopic bond orientation model *J. Electr. Spectrosc. Relat. Phenom.* **98** 189
- [34] Stöhr J 1999 Exploring the microscopic origin of magnetic anisotropies with x-ray magnetic circular dichroism (XMCD) spectroscopy *J. Magn. Magn. Mater.* **200** 470
- [35] Weser M, Rehder Y, Horn K, Sicot M, Fonin M, Preobrajenski A B, Voloshina E N, Goering E and Dedkov Yu S 2010 Induced magnetism of carbon atoms at the graphene/Ni(111) interface *Appl. Phys. Lett.* **96** 012504
- [36] Brühwiler P A, Maxwell A J, Puglia C, Nilson A, Anderson S and Mårtensson N 1995  $\pi^*$  and  $\sigma^*$  excitons in C 1s absorption of graphite *Phys. Rev. Lett.* **74** 614
- [37] Ahuja R, Brühwiler P A, Wills J M, Johansson B, Mårtensson N and Eriksson O 1996 Theoretical and experimental study of the graphite 1s x-ray absorption edges *Phys. Rev. B* **54** 14396
- [38] Wessely O, Katsnelson M I and Eriksson O 2005 *Ab initio* theory of dynamical core-hole screening in graphite from x-ray absorption spectra *Phys. Rev. Lett.* **94** 167401
- [39] Preobrajenski A B, Ng M L, Vinogradov A S and Mårtensson N 2008 Controlling graphene corrugation on lattice-mismatched substrates *Phys. Rev. B* **78** 073401
- [40] Eom D, Prezzi D, Taeg Rim K, Zhou H, Lefenfeld M, Xiao S, Nuckolls C, Hybertsen M S, Heinz T F and Flynn G W 2009 Structure and electronic properties of graphene nanoislands on Co(0001) *Nano. Lett.* **9** 2844
- [41] Srivastava P, Wilhelm F, Ney A, Farle M, Wende H, Haack N, Ceballos G and Baberschke K 1998 Magnetic moments and Curie temperatures of Ni and Co thin films and coupled trilayers *Phys. Rev. B* **58** 5701
- [42] Dhesi S S, Dürr H A, van der Laan G, Dudzik E and Brookes N B 1999 Electronic and magnetic structure of thin Ni films on Co/Cu(001) *Phys. Rev. B* **60** 12852
- [43] Nesvizhskii A I, Ankudinov A L, Rehr J J and Baberschke K 2000 Interpretation of x-ray magnetic circular dichroism and x-ray absorption near-edge structure in Ni *Phys. Rev. B* **62** 15295
- [44] Thole B T, Carra P, Sette F and van der Laan G 1992 X-ray circular dichroism as a probe of orbital magnetization *Phys. Rev. Lett.* **68** 1943

- [45] Carra P, Thole B T, Altarelli M and Wang X D 1993 X-ray circular dichroism and local magnetic fields *Phys. Rev. Lett.* **70** 694
- [46] Huang D J *et al* 2002 Orbital magnetic moments of oxygen and chromium in CrO<sub>2</sub> *Phys. Rev. B* **66** 174440
- [47] Sorg C, Ponpandian N, Scherz A, Wende H, Nunthel R, Gleitsmann T and Baberschke K 2004 The magnetism of ultrathin Ni films grown with a surfactant *Surf. Sci.* **565** 197
- [48] Baberschke K 1996 The magnetism of nickel monolayers *Appl. Phys. A* **62** 417
- [49] Yamamoto K, Fukushima M, Osaka T and Oshima C 1992 Charge-transfer mechanism for the (monolayer graphite)–Ni(111) system *Phys. Rev. B* **45** 11358
- [50] Mertins H, Valencia S, Gudat W, Oppeneer P, Zaharko O and Grimmer H 2004 Direct observation of local ferromagnetism on carbon in C/Fe multilayers *Europhys. Lett.* **66** 743
- [51] Céspedes O, Ferreira M S, Sanvito S, Kociak M and Coey J M D 2004 Contact induced magnetism in carbon nanotubes *J. Phys.: Condens. Matter* **16** L155
- [52] Sorg C, Ponpandian N, Bernien M, Baberschke K, Wende H and Wu R Q 2006 Induced magnetism of oxygen in surfactant-grown Fe, Co, and Ni monolayers *Phys. Rev. B* **73** 064409
- [53] Rader O, Varykhalov A, Sanchez-Barriga J, Marchenko D, Rybkin A and Shikin A M 2009 Is there a Rashba effect in graphene on 3d ferromagnets? *Phys. Rev. Lett.* **102** 057602
- [54] Shikin A M, Prudnikova G V, Adamchuk V K, Moresco F and Rieder K H 2000 Surface intercalation of gold underneath a graphite monolayer on Ni(111) studied by angle-resolved photoemission and high-resolution electron-energy-loss spectroscopy *Phys. Rev. B* **62** 13202
- [55] Grüneis A and Vyalikh D 2008 Tunable hybridization between electronic states of graphene and a metal surface *Phys. Rev. B* **77** 193401